coatings

MDPI

Article

Plasma Carburizing of Laser Powder Bed Fusion Manufactured 316 L Steel for Enhancing the Surface Hardness

Roberto Montanari [1,*], Alex Lanzutti [2], Maria Richetta [1], Javokhir Tursunbaev [1], Emanuele Vaglio [2], Alessandra Varone [1] and Claudio Verona [1]

[1] Department of Industrial Engineering, University of Rome "Tor Vergata", Via del Politecnico 1, 00133 Roma, Italy; richetta@uniroma2.it (M.R.); mr.tursunboyev@gmail.com (J.T.); alessandra.varone@uniroma2.it (A.V.); claudio.verona@uniroma2.it (C.V.)

[2] Polytechnic Department of Engineering and Architecture, University of Udine, Via delle Scienze 208, 33100 Udine, Italy; alex.lanzutti@uniud.it (A.L.); emanuele.vaglio@uniud.it (E.V.)

* Correspondence: roberto.montanari@uniroma2.it

Abstract: Austenitic stainless steels produced by laser powder bed fusion (L-PBF) are quite interesting materials owing to their specific microstructure consisting of dendrite walls built of dislocations pinned by many nano-oxides that involves significant strengthening without loss of ductility. In this work, different plasma treatments were performed to harden the surface of 316 L steel manufactured by L-PBF. The samples were characterized by X-ray diffraction (XRD), Raman spectroscopy (RS), light microscopy (LM) and micro-hardness tests. The experimental results show that all the plasma treatments enhance the hardness of the surface because a C-enriched layer of austenite (S-phase) forms with a thickness up to 25 µm. The plasma gas mixture, consisting of 2.5% (CH_4) + 97.5% (H_2), resulted in being the most effective and produced a surface hardness (547 ± 27 HV) more than double with respect to that of the untreated material. The treatment temperature was 475 °C, which represents a good compromise between the necessity to avoid the precipitation of $M_{23}C_6$ carbides and the compatibility of treatment time with the industrial practice. Moreover, it has been observed that a 2 µm-thick over-layer of amorphous C forms on the sample surface. The hardness of such over-layer, which depends on the specific treatment and is related to the degree of topological disorder, is generally greater than that of S-phase. The work demonstrates that plasma carburizing is quite effective in hardening the surface of 316 L steel manufactured by L-PBF and further improves its mechanical properties, which are basically superior to those of the same material prepared by conventional processes.

Keywords: austenitic stainless steels; 316 L steel; additive manufacturing; laser powder bed fusion; low temperature carburizing; plasma treatment; microstructural characterization

Citation: Montanari, R.; Lanzutti, A.; Richetta, M.; Tursunbaev, J.; Vaglio, E.; Varone, A.; Verona, C. Plasma Carburizing of Laser Powder Bed Fusion Manufactured 316 L Steel for Enhancing the Surface Hardness. *Coatings* **2022**, *12*, 258. https://doi.org/10.3390/coatings12020258

Academic Editor: Cheng Zhang

Received: 21 January 2022
Accepted: 13 February 2022
Published: 15 February 2022

1. Introduction

Owing to their excellent corrosion resistance, austenitic stainless steels are commonly used in several industrial sectors (chemical, pharmaceutical, biomedical, food etc.). In spite of recent improvements achieved by additive manufacturing [1], low hardness and wear resistance still represent an intrinsic limit to the different applications. Unfortunately, for these materials, conventional thermo-chemical surface treatments, such as carburizing, nitriding and carbo-nitriding, are not helpful. Since these treatments are usually performed at temperatures higher than 550 °C, they induce the precipitation of Cr carbides with consequent Cr depletion of the surrounding matrix, therefore the improvement of hardness takes place with detrimental effects on corrosion resistance.

To overcome these problems, a lot of work has been undertaken in the last 20 years for developing thermo-chemical treatments at lower temperature [2]. They are carried out at atmospheric pressure and temperature in the range 350–550 °C, where C diffusion is slow; thus, the exposed metal surface needs to be activated by removing the passive

layer of Cr_2O_3 that represents the main obstacle to C penetration. Among low temperature treatments, kolsterizing is one of the most efficient [3]: a pre-treatment in gaseous HCl atmosphere at ~250 °C removes Cr_2O_3 from the surface of the austenitic stainless steel, then it is treated at ~450 °C for about 30 h in an atmosphere of CO, H_2 and N_2. Owing to C supersaturation, a layer of expanded austenite (S-phase) forms with thickness of ~30 μm and both mechanical and corrosion resistance results improved [4–7]. Young's modulus [8,9] and hardness [2] of S-phase are greater than those of austenite and exhibit a decreasing trend with the distance from the surface depending on the amount of interstitial C in austenite lattice. Such microstructural characteristics lead to a remarkable enhancement of wear resistance [10–12], also in temperatures up to 600 °C [13]. Another advantage of kolsterizing treatment consists in the strong compressive stresses (up to 2 GPa) of the S-phase which hinder crack propagation and contribute to improve fatigue resistance [14]. Moreover, f.c.c. structure guarantees good ductility of the hardened layer [15].

The precipitation of carbides does not occur if the C concentration at the surface does not exceed 12%, whereas above this value metastable M_5C_2 carbides have been observed in the steel matrix [3,16].

In spite of its relevant advantages, kolsterizing involves a long treatment time with resulting high costs. On the basis of this consideration, a plasma-assisted carburizing process at low temperature was developed by us [6,7] some years ago to reduce treatment time, as well as lower the costs. Such plasma process, applied to 316 L steel, exploited the superior chemical reactivity of the highly ionized gas and the greater collision energy. The process resulted in being effective, even if it is of difficult application to mechanical parts of large size and complex shape.

Today, new interest arises from the development and evolution of additive manufacturing [17,18], a technology gaining increasing importance in industrial and academic fields. It allows for the production of components of different alloys and among them the austenitic stainless steels have been extensively investigated [19–25] owing to their specific microstructure (dendrite walls built of dislocations pinned by many nano-oxides) involving significant strengthening without loss of ductility.

The aim of this work is to investigate the plasma treatment on L-PBF manufactured steel samples and find the best process conditions for enhancing the surface hardness. The attention has been mainly focused on the gas mixture that represents the most critical parameter of plasma carburizing process. Seven different treatments have been carried out and all the samples examined by X-ray diffraction (XRD), Raman spectroscopy (RS), light microscopy (LM) and micro-hardness tests.

2. Materials and Methods

2.1. Samples

The investigated material is the AISI 316 L steel manufactured by L-PBF; its nominal chemical composition is the following: C 0.024, N 0.083, Mn 1.35, Si 0.40, Cr 16.87, Ni 10.05, Mo 2.06, P 0.031, S 0.029, Fe to balance (wt.%).

The 3D printed samples were obtained by using commercial powders with particles of spherical shape and a granulometric distribution in the range 18.17 μm (10th %ile)–45.44 μm (90th %ile), with a median particle diameter of 28.72 μm. The samples were manufactured using a Concept Laser M2 Cusing machine equipped with a single-mode CW ytterbium-doped fiber laser with an emission wavelength of 1070 nm. The process was performed in Ar atmosphere with O partial pressure lower than 0.2%. The main L-PBF process parameters were the following: power 180 W, scanning speed 600 mm/s, spot diameter 120 μm, hatch distance 105 μm, layer thickness 25 μm.

The parts were processed according to the island exposure strategy, producing a checkerboard pattern consisting of 5×5 mm^2 squares obtained by bi-directionally scanning consecutive single tracks. The adjacent islands were allowed to overlap each other by 105 μm and were scanned along mutually perpendicular directions. The islands were rotated by 90° and moved by 1 mm along the X and Y directions for the production

of each subsequent layer (Figure 1a). A total of 20 specimens oriented parallel to the building platform were prepared with a size of 30.5 × 20.5 × 7 mm^3 (Figure 1b). More details about sample manufacturing are given in reference [26]. As also reported by other investigators [27–29], after L-PBF manufacturing the structure of the steel consists of austenite plus ~5% of δ-ferrite.

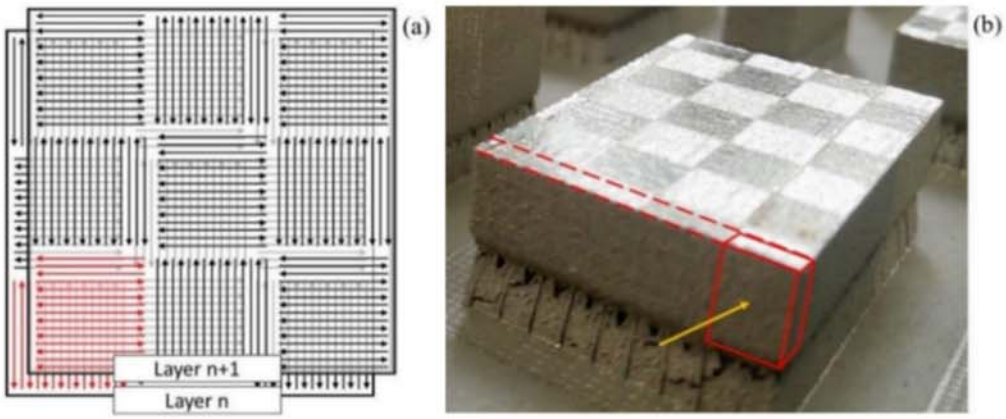

Figure 1. Island exposure strategy (**a**) and a piece produced by L-PBF (**b**). A typical sample used for plasma treatments, shown in (**b**) by continuous red lines, was obtained from slices (dashed red line) cut perpendicularly to the built surface. The surface exposed to plasma is indicated by the yellow arrow.

The samples used in present experiments had the following dimensions: length 7 mm, width 6 mm, thickness 2 mm. As schematically shown in Figure 1b, they were obtained from slices (2 mm thick) cut perpendicularly to the built surface by using a diamond saw. The samples were at first mechanically polished through grinding papers and a suspension of 0.3 μm alumina powder in water to get a mirror-like surface; then, they were immersed in a sonication bath for 10 min.

2.2. Plasma Treatments

The passive oxidation layer was at first removed from the surface by means of hydrogen bombardment for a duration of 15 min carried out in the vacuum chamber used for plasma treatments. The surface indicated by the yellow arrow in Figure 1b has been then exposed to the plasma. The treatments were performed using a microwave plasma enhanced Chemical Vapour Deposition (CVD) reactor [30]. A schematic view of the experimental set-up is shown in Figure 2. The vacuum chamber (background pressure of 10–5 mbar) is a quartz tube where different gases, i.e., H_2, CH_4 and CO_2, flow by flowmeters at a stationary fixed pressure of 70 mbar. The purity of CH_4, H_2 and CO_2 gases are 99.9995%, 99.9999% and 99.9995%, respectively. The quartz tube is placed across a waveguide connected to a commercial 2.45 GHz microwave generator. The microwave power was set in the range 400–500 W. Microwaves give energy to the electrons of the plasma, which transfer energy to the gas through molecular collisions, heating it. The temperature of the steel sample was monitored by means of an infrared optical pyrometer. According to the time-temperature-transformation (TTT) diagram in Figure 3, plasma treatments were performed at a temperature of 475 °C to avoid the precipitation of $M_{23}C_6$ carbides and η, χ and σ phases. The chemical and physical reactions, which follow this heating, allow the formation of a C rich layer on the steel surface. The gas mixture compositions and temperature used during the plasma treatments are reported in Table 1. The duration of each treatment was 7 h.

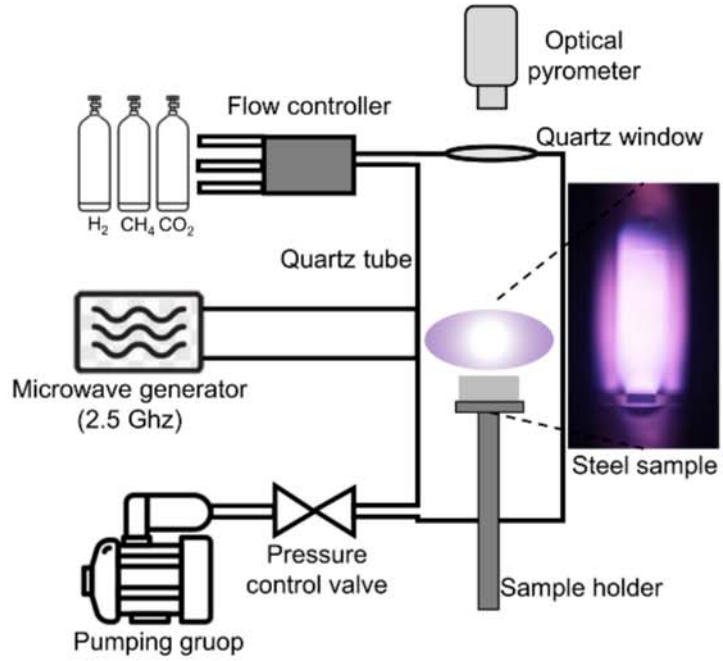

Figure 2. Schematic view of the experimental set-up used for plasma treatments.

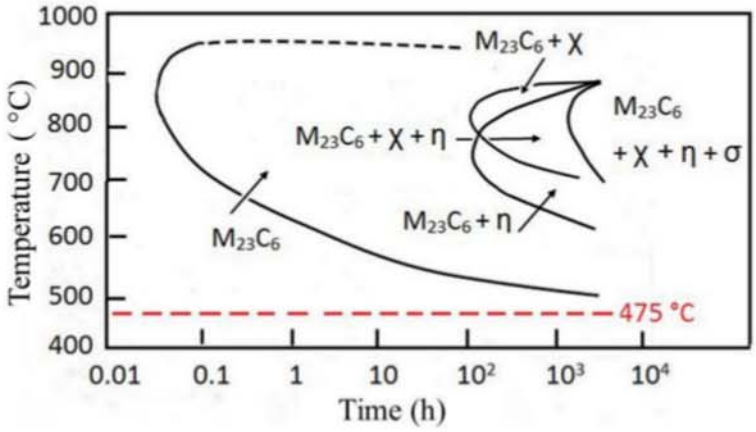

Figure 3. TTT diagram of austenitic stainless steels.

Table 1. Gas mixture and temperature used for treating different groups of samples.

Samples	Gas Mixture	Treatment Temperature
#1	0.5%(CH_4) + 99.5%(H_2)	475 °C
#2	1%(CH_4) + 99%(H_2)	475 °C
#3	2%(CH_4) + 98%(H_2)	475 °C
#4	2.5%(CH_4) + 97.5%(H_2)	475 °C
#5	4%(CH_4) + 96%(H_2)	475 °C
#6	4%(CO_2) + 96%(H_2)	475 °C
#7	2.5%(CH_4) +1.5%(CO_2) +96%(H_2)	475 °C

As reported in Table 1, a series of plasma treatments was performed at 475 °C by varying the composition of the CH_4 + H_2 gas mixture (samples from #1 to #5), and other two gas mixtures were tested by adding CO_2 (samples #6 and #7).

2.3. Sample Characterization

XRD measurements (Philips, Eindhoven, Netherlands) have been carried out by using the Mo-Kα radiation (λ = 0.071 nm). Diffraction patterns have been collected in the 2θ angular range 15°–50° in step-scanning mode with 2θ steps of 0.05° and counting time per step of 5 s. High precision peak profiles of the most intense XRD reflections have been recorded with 2θ steps of 0.005° and counting time per step of 10 s. The lattice parameters of austenite before ($\alpha_{0\gamma}$) and after (α_{γ}) plasma treatments have been determined by using the $\cos^2\theta$ method [31], and from these values the carbon content C_{γ} (wt.%) in the S phase has been then estimated through the relationship:

$$\alpha_{\gamma} = \alpha_{0\gamma} + \alpha C_{\gamma}, \quad (1)$$

where α is a constant (0.0044 nm/wt.% C) empirically determined by Ridley et al. [32].

Vickers micro-hardness tests (micro-hardness tester Shimadzu corporation, Kyoto, Japan) were performed on the treated surfaces by applying a load of 1000 g for a time of 10 s. For each group of samples, 15 micro-hardness tests were made to determine the mean hardness value of the treated surfaces and the standard deviation. Hardness profiles vs. the distance from the surface were also made on cross-sections of the samples by using a lower load (25 g) to get a better spatial resolution.

3. Results and Discussion

The LM micrographs in Figure 4 show the structure of the 316 L steel prepared by L-PBF. In the sample top view (Figure 4a), the laser tracks rotated of 90° during building process are clearly visible, while the melting pools can be observed in the cross-section (Figure 4b).

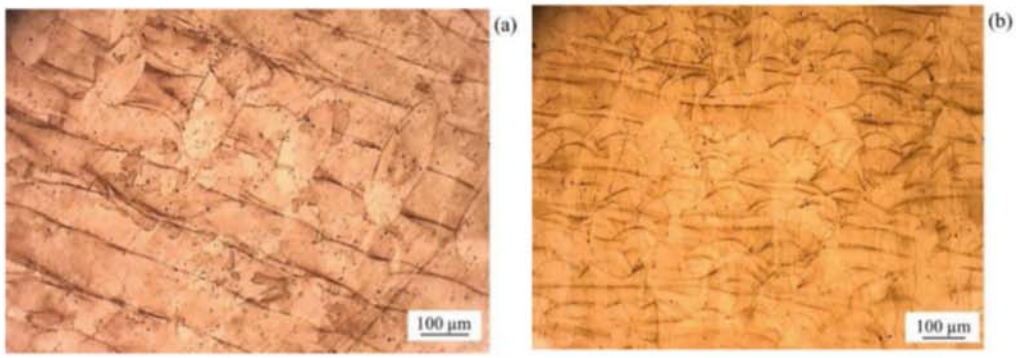

Figure 4. Top view (**a**) and cross-section (**b**) of 316 L steel manufactured by L-PBF process.

All the plasma treatments listed in Table 1 give rise to a surface layer of S-phase on the exposed surface with thickness ranging from 20 to 25 µm. For example, Figure 5 shows the cross-sections of samples #2 (Figure 5a) and #5 (Figure 5b), and in both the micrographs the layer of S-phase can be easily identified by the brighter colour. In Figure 5c the cross-section of the untreated material is displayed for comparison.

Table 2 reports the micro-hardness measured with a load of 1000 g on the exposed surface of samples submitted to plasma treatments in different conditions. For all the examined samples, the hardness is always greater than that of untreated austenite (HV = 245 ± 3).

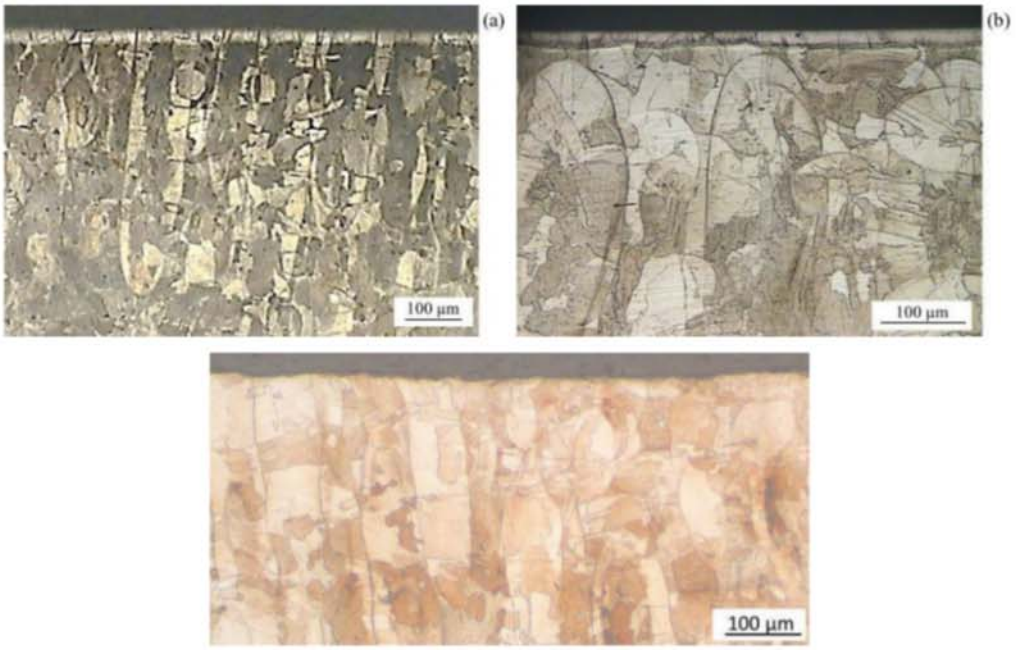

Figure 5. Cross-sections of the samples #2 (**a**) and #5 (**b**). The S-phase layer covers the exposed surface. In (**c**) the untreated material is displayed for comparison.

Table 2. Hardness measured with a load of 1000 g on the exposed surface after plasma treatments in different conditions. For comparison the hardness values of untreated L-PBF steel and 316 L steel manufactured by forging are reported too.

Samples	Gas Mixture	HV_1
#1	0.5% (CH_4) + 99.5% (H_2)	450 ± 13
#2	1% (CH_4) + 99% (H_2)	467 ± 10
#3	2% (CH_4) + 98% (H_2)	534 ± 36
#4	2.5% (CH_4) + 97.5% (H_2)	547 ± 27
#5	4% (CH_4) + 96% (H_2)	421 ± 21
#6	4% (CO_2) + 96% (H_2)	269 ± 4
#7	2.5% (CH_4) + 1.5% (CO_2) + 96% (H_2)	469 ± 12
L-PBF	No plasma treatment	245 ± 3
Forged 316 L	No plasma treatment	147 ± 2

By comparing data of samples #5 and #6 in Table 2, it is evident that CH_4 is more effective than CO_2 to harden the steel surface. In the case of samples from #1 to #5 treated with CH_4 + H_2 in various fractions, the best result in terms of absolute hardness (HV = 547 ± 27) and thickness of hardened layer (~25 µm) is obtained by using a gas mixture containing 2.5% of CH_4 (sample #4), namely, an intermediate fraction among those experimented here. It is reasonable that higher amounts of CH_4 in gas mixture may induce the precipitation of fine carbides, as already reported for similar treatments carried out on conventional 316 L steel [6]. This seems also in agreement with the greater hardness of sample #7 compared to sample #5. From the present results, the treatment temperature of 475 °C seems to represent a good compromise between the necessity to avoid the precipitation of $M_{23}C_6$ carbides and the compatibility of treatment time with the industrial practice.

Figure 6 shows that the hardness of all the samples progressively decreases with the distance from the surface. The hardness profiles depend on the specific treatment, but some variations have been observed also in the same sample. Seven profiles have been measured for each sample and those displayed in the figure are the most representative.

The result suggests that plasma-sample coupling is not perfectly homogeneous on the whole exposed surface.

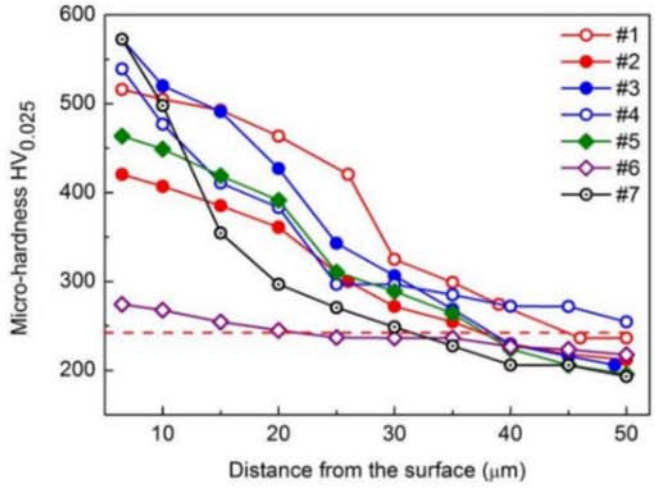

Figure 6. Micro-hardness (load of 25 g) profiles vs. distance from the exposed surface of 316 L samples treated in different conditions.

It is also observed that hardening in the major part of samples takes place in a more extended zone (up to a depth of 30–35 μm) than that evidenced by LM micrographs (Figure 5). Moreover, except #1 and #4, all the other samples exhibit hardness a little lower than that of untreated austenite at a depth larger than ~40 μm, likely due to recovery of lattice defects.

XRD measurements carried out on the treated samples show that all the peaks are shifted towards lower angles. Figure 7 compares the {110} and {200} reflections of the steel before and after plasma treatments: the relevant shift of both the peaks is connected to the austenite expansion induced by the excess of C in lattice interstitial positions.

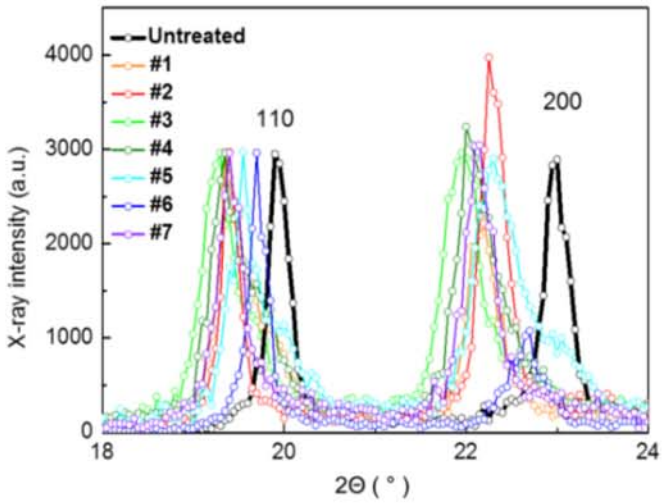

Figure 7. {110} and {200} XRD reflections of 316 L steel prepared by L-PBF before and after plasma treatments. After plasma treatments, the peaks shift towards lower angles due to the expansion of austenite lattice.

From XRD measurements, the lattice parameter of S-phase in different samples has been determined and the C content calculated by means of Equation (1). The C content in S-phase varies with gas mixtures and the highest value has been detected in samples #3, treated by using a gas mixture made of 2% (CH_4) + 98% (H_2) at 475 °C.

Hardness of S-phase is expected to linearly increase with C content; however, the plot in Figure 8 displays a significant scattering of data with respect such trend. This suggests that hardness could be affected by the presence of a C-rich over-layer, as previously observed in plasma treatments carried out on the same material manufactured by cold rolling [6]. To assess such occurrence, Vickers micro-hardness tests were performed on the plasma exposed surfaces by applying different loads from 25 to 1000 g. Under these conditions, the indentation depth is of several microns; thus, the indentation size effect (ISE) can be neglected [33,34]. In the case of a homogeneous material, micro-hardness does not depend on the load used in the test. On the contrary, if the tests are carried out on a surface coated by a thin layer with characteristics different from those of the substrate, micro-hardness changes with the applied load because greater loads lead to deeper penetration of the indenting tip, namely different amounts of coating and substrate are involved in the tests. Many methods using this approach for determining the hardness of thin coatings are reported in the literature [35] and applied to a large variety of materials (e.g., see references [36,37]). The results of present experiments are shown in Figure 9, where the mean micro-hardness values are plotted vs. penetration depth. The points in each curve correspond to the values measured in tests carried out by using loads of 25, 50, 100, 300, 500 and 1000 g.

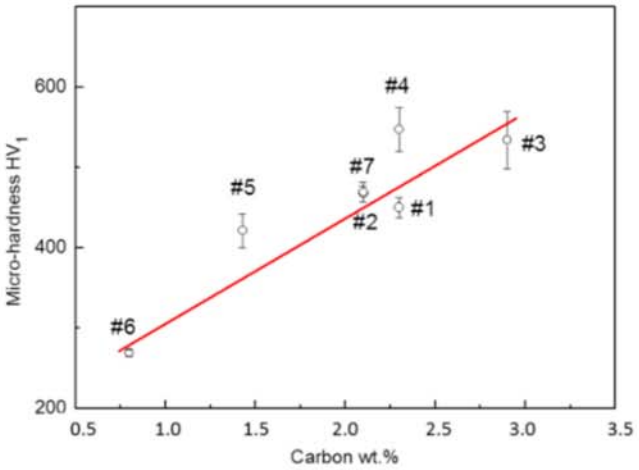

Figure 8. Micro-hardness vs. C content determined in different samples through XRD. Micro-hardness values were obtained by applying a load of 1000 g.

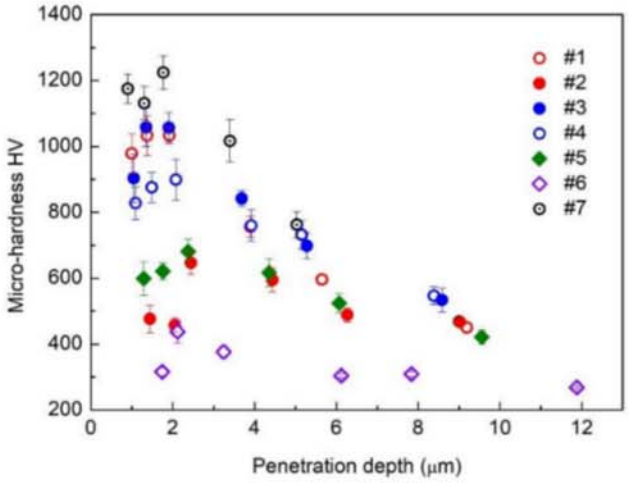

Figure 9. Micro-hardness vs. penetration depth. The tests have been carried out on the plasma exposed surface by using 6 different loads (25, 50, 100, 300, 500 and 1000 g). Each point in the curves corresponds to a specific load.

It is evident from Figure 9 that the measured micro-hardness values strongly depend on the load used in the test. Within the experimental error, micro-hardness values can be considered substantially constant up to a penetration depth of ~2 μm, while relevant variations are observed for larger penetration depths. As schematically displayed in Figure 10a, for loads lower than 100 g, the indenting tip penetrates only the over-layer that results in having a thickness of ~2 μm, and the measured micro-hardness value basically corresponds to that of the over-layer. For applied loads greater than 100 g, the tests also involve the S-phase (Figure 10b); thus, the value obtained by the test depends on the hardness of both over-layer and S-phase. Of course, as load increases, the volume of S-phase involved in the test becomes progressively more relevant and, consequently, its effect on the measured value.

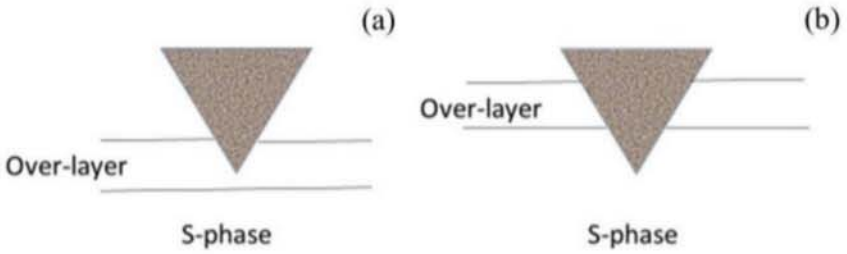

Figure 10. Schematic view of the indenter tip penetrating only the hard over-layer for lower loads (**a**) and also the S-phase for greater loads (**b**). The over-layer thickness resulted to be ~2 μm.

Another significant piece of information provided by Figure 9 is that the hardness of the over-layer exhibits large variations after different treatments; thus, it is important to identify its nature and characteristics. In a previous work [6] a similar C-rich graphitic over-layer has been observed in cold rolled 316 L steel after plasma treatments. Gas mixtures (H_2/CH_4) are commonly employed to grow synthetic polycrystalline diamond films and the addition of CO_2 is demonstrated to enhance the growth rate and crystalline quality of nano-diamond layers [38–40]. The reason why meta-stable diamond crystals can nucleate and grow on non-diamond substrates under CVD conditions is a problem that has been extensively debated (e.g., see [41–45]) since the most stable C phase is graphite and the phase transition has a high activation barrier (~0.4 eV/atom) that can be overcome under extreme conditions of temperature and pressure. A model for diamond nucleation by energetic species was proposed by Lifshitz et al. [41]; it involves spontaneous bulk nucleation of diamond embryo clusters in an amorphous carbon hydrogenated matrix and ion bombardment-induced growth through a preferential displacement mechanism. The model has been confirmed by TEM observations of Li et al. [45].

To identify the specific nature of the over-layer, Raman spectra have been collected. RS is a sensitive technique for identifying the variety of crystalline and amorphous C structures that may exist in different hybridization states [46,47].

Figure 11 clearly shows that two peaks, i.e., the D-band and G-band peaks, are present in the RS patterns of the samples from #1 to #5, treated at 475 °C with a gas mixture containing CH_4 and H_2 in various fractions, and of sample #7. On the contrary, the peaks are very weak, at the limit of detectability, in the case of the sample #6 treated with 4% (CO_2) + 96% (H_2), a gas mixture without CH_4. The RS of untreated (UT) sample is also reported in Figure 11 for comparison. The diamond peak at 1332 cm^{-1}, whose position is indicated by the dashed vertical line in Figure 11, was never observed.

The G and D peaks are due to sp^2 sites and correspond to neighbour atoms moving in opposite directions perpendicular to the plane of the graphitic sheet (G peak) or in radial directions in the plane (D peak). The presence of the D peak indicates a topological disorder into the graphite layer even if bonding is still sp^2; therefore, the ratio I_D/I_G between the intensities of D and G peaks can be used evaluate the degree of disorder.

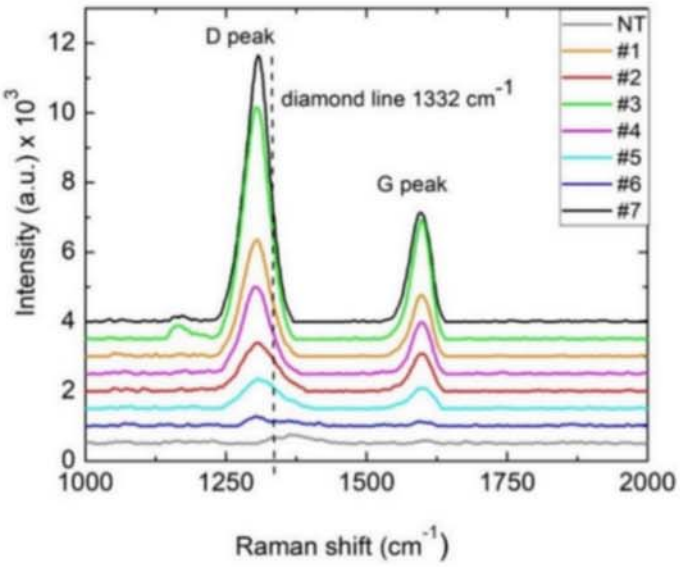

Figure 11. Raman spectra of the samples in original state (NT) and treated with plasma in different conditions. The position (1332 cm^{-1}) of the peak of diamond single crystal, indicated by the dashed vertical line, is displayed for comparison.

Figure 11 shows that the relative intensities of D and G peaks vary with the specific treatment. For the samples treated at 475 °C with different mixtures of CH_4 and H_2 (from #1 to #5) I_D/I_G decreases from 1.93 (sample #3) to 1.68 (sample #5), and this corresponds to a decrease in the over-layer hardness (first points of the curves in Figure 9). Therefore, over-layer hardness seems related to the disorder degree. This is also supported by the data of sample #7, which has an extremely hard (~1100 HV) over-layer and the greatest value of the ratio (I_D/I_G = 2.47) among those of all the curves reported in Figure 9. Anyway, to assess such a hypothesis, X-ray photoelectron spectroscopy (XPS) measurements are underway.

On the basis of RS results, the anomalous scattering of micro-hardness data vs. C content in S-phase (Figure 8) can be explained by the different depth of analysis of XRD and micro-hardness tests. XRD examines the material at a depth in the range of 40–50 μm and the effect of the over-layer (2 μm thick) is negligible whereas the penetration depth of the tip in micro-hardness tests with an applied load of 1000 g is ~10–12 μm, thus is more sensitive to the over-layer hardness.

4. Conclusions

The work investigated seven plasma treatments on 316 L steel manufactured by L-PBF to find the best process conditions for enhancing the surface hardness. The samples were examined using XRD, RS, LM and micro-hardness tests, and the results were précised as follows:

1. All the plasma treatments enhance the hardness of the 316 L steel, owing to the formation of a C-enriched layer of austenite (S-phase) with thickness ranging from 20 to 25 μm.
2. The layer of S-phase exhibits a hardness profile decreasing toward the inner part of material depending to the C diffusion profile.
3. Among the different gas mixtures used in present experiments for producing the plasma, that consisting of 2.5% (CH_4) + 97.5% (H_2) resulted in being the most effective: the surface hardness becomes 547 ± 27 HV, more than double if compared to that of the original steel manufactured by L-PBF (HV = 245 ± 3).
4. The treatment temperature of 475 °C represents a good compromise between the necessity to avoid the precipitation of $M_{23}C_6$ carbides and the compatibility of treatment time with the industrial practice.

5. A 2 μm-thick over-layer of amorphous C forms on the sample surface. The hardness of this over-layer changes with the specific treatment, but it is generally greater than that of S-phase. Raman spectra suggest that over-layer hardness is related to the degree of topological disorder, described by the ratio I_D/I_G between the intensities of D and G peaks.

In conclusion, plasma carburizing is quite effective in hardening the surface of 316 L steel manufactured by L-PBF and further improves its mechanical properties, which are basically superior to those of the same material prepared by conventional processes such as cold rolling and forging. In the future, wear tests will be carried out to assess whether the increase in hardness is accompanied by an improvement of tribological properties.

Author Contributions: R.M. and A.V. planned the experiments; A.L. and E.V. prepared the samples by L-PBF; C.V. carried out plasma treatments and Raman experiments, A.V., M.R. and J.T. performed the microstructural characterization and micro-hardness tests; all the authors contributed to analyze the results; R.M. and A.V. wrote the manuscript. All authors have read and agreed to the published version of the manuscript.

Funding: This research received no external funding.

Institutional Review Board Statement: Not applicable.

Informed Consent Statement: Not applicable.

Data Availability Statement: Not applicable.

Acknowledgments: The authors are grateful to Piero Plini and Emanuela Sgreccia of Department of Industrial Engineering—University of Rome "Tor Vergata" for the assistance in sample preparation and Raman measurements. The Laboratory for Advanced Mechatronics—LAMA FVG—of the University of Udine is also gratefully acknowledged, in particular M. Sortino and G. Totis. LAMA FVG is an international research centre for product and process innovation where the three Universities of Friuli Venezia Giulia Region (Italy) synergically cooperate for promoting Research and Development activities at academic and industrial level.

Conflicts of Interest: The authors declare no conflict of interest.

References

1. Bartolomeu, F.; Buciumeanu, M.; Pinto, E.; Alves, N.; Carvalho, O.; Silva, F.S.; Miranda, G. 316L stainless steel mechanical and tribological behavior—A comparison between selective laser melting, hot pressing and conventional casting. *Addit. Manuf.* **2017**, *16*, 81–89. [CrossRef]
2. Collins, S.R.; Williams, P.C.; Marx, S.V.; Heuer, A.; Ernst, F.; Kahn, H. Low-temperature carburization of austenitic stainless steels. In *ASM Handbook, Heat Treating of Irons and Steels*; Dossett, J., Totten, G.E., Eds.; ASM International: Almere, The Netherlands, 2014; Volume 4D, pp. 451–460.
3. Collins, S.R.; Williams, P.C. Low-temperature colossal supersaturation. *Adv. Mater. Process* **2006**, *164*, 32–33.
4. Michal, G.M.; Ernst, F.; Kahn, H.; Cao, Y.; Oba, F.; Agarwal, N.; Heuer, A.H. Carbon supersaturation due to paraequilibrium carburisation: Stainless steels with greatly improved mechanical properties. *Acta Mater.* **2006**, *54*, 1597–1606. [CrossRef]
5. Gentil, J.; Ernst, F.; Michal, G.; Heuer, A. The effect of colossal carbon supersaturation on stainless steels of the type PH13-8Mo and AL6XN, MS&T 2006. In Proceedings of the Materials Science & Technology Conference, Cincinnati, OH, USA, 15–19 October 2006.
6. Ciancaglioni, I.; Donnini, R.; Kaciulis, S.; Mezzi, A.; Montanari, R.; Ucciardello, N.; Verona-Rinati, G. Surface modification of austenitic steels by low temperature carburization. *Surf. Interface Anal.* **2012**, *44*, 1001–1004. [CrossRef]
7. Balijepalli, S.K.; Ceschini, L.; Ciancaglioni, I.; Kaciulis, S.; Mezzi, A.; Montanari, R.; Martini, C.; Verona Rinati, G. Corrosion effect to the surface of stainless steel treated by two processes of low temperature carburization. *Surf. Interface Anal.* **2014**, *46*, 731–734. [CrossRef]
8. Balijepalli, S.K.; Colantoni, I.; Donnini, R.; Kaciulis, S.; Lucci, M.; Montanari, R.; Ucciardello, N.; Varone, A. Modulo elastico della fase S in un acciaio 316 L kolsterizzato. *La Metall. Ital.* **2013**, *1*, 42–47.
9. Balijepalli, S.K.; Donnini, R.; Kaciulis, S.; Montanari, R.; Varone, A. Young's modulus profile in kolsterized AISI 316 L steel. *Mater. Sci. Forum* **2013**, *762*, 183–188. [CrossRef]
10. Qu, J.; Blau, P.J.; Jolly, B.C. Tribological properties of stainless steels treated by colossal carbon supersaturation. *Wear* **2007**, *263*, 719–726. [CrossRef]
11. Sun, Y. Tribocorrosion behavior of low temperature plasma carburized stainless steel. *Surf. Coat. Technol.* **2013**, *228*, S342–S348. [CrossRef]

12. Ceschini, L.; Chiavari, C.; Lanzoni, E.; Martini, C. Low-temperature carburised AISI 316 L austenitic stainless steel: Wear and corrosion behavior. *Mater. Des.* **2012**, *38*, 154–160. [CrossRef]
13. Rotundo, F.; Ceschini, L.; Martini, C.; Montanari, R.; Varone, A. High temperature tribological behaviour and microstructural modifications of the low-temperature carburised AISI 316 L austenitic stainless steel. *Surf. Coat. Technol.* **2014**, *258*, 772–781. [CrossRef]
14. Agarwal, N.; Kahn, H.; Avishai, A.; Heuer, A.; Michal, G.; Ernst, F. Enhanced fatigue resistance in 316L austenitic stainless steel due to low-temperature paraequilibrium carburization. *Acta Mater.* **2007**, *55*, 5572–5580. [CrossRef]
15. Sun, Y.; Chin, L.Y. Residual stress evolution and relaxation in carbon S phase layers on AISI 316 austenitic stainless steel. *Surf. Eng.* **2002**, *18*, 443–446. [CrossRef]
16. Ernst, F.; Cao, Y.; Michal, G.M.; Heuer, A.H. Carbide precipitation in austenitic stainless steel carburized at low temperature. *Acta Mater.* **2007**, *55*, 1895–1906. [CrossRef]
17. Herzog, D.; Seyda, V.; Wycisk, E.; Emmelmann, C. Additive manufacturing of metals. *Acta Mater.* **2016**, *117*, 371–392. [CrossRef]
18. Huang, S.H.; Liu, P.; Mokasdar, A.; Huo, L. Additive manufacturing and its societal impact: A literature review. *Int. J. Adv. Manuf. Technol.* **2013**, *67*, 1191–1203. [CrossRef]
19. Bajaj, P.; Hariharan, A.; Kini, A.; Kürnsteiner, P.; Raabe, D.; Jägle, E.A. Steels in additive manufacturing: A review of their microstructure and properties. *Mater. Sci. Eng. A* **2020**, *772*, 138633. [CrossRef]
20. Wang, Y.M.; Voisin, T.; McKeown, J.T.; Ye, J.; Calta, N.P.; Li, Z.; Zeng, Z.; Zhang, Y.; Chen, W.; Roehling, T.T.; et al. Additively manufactured hierarchical stainless steels with high strength and ductility. *Nat. Mater.* **2018**, *17*, 63–70. [CrossRef]
21. Khodabakhshi, F.; Farshidianfar, M.H.; Gerlich, A.P.; Nosko, M.; Trembošová, V.; Khajepour, A. Effects of laser additive manufacturing on microstructure and crystallographic texture of austenitic and martensitic stainless steels. *Addit. Manuf.* **2019**, *31*, 100915. [CrossRef]
22. Chen, N.; Ma, G.; Zhu, W.; Godfrey, A.; Shen, Z.; Wu, G.; Huang, X. Enhancement of an additive-manufactured austenitic stainless steel by post-manufacture heat-treatment. *Mater. Sci. Eng. A* **2019**, *759*, 65–69. [CrossRef]
23. Kong, D.; Dong, C.; Ni, X.; Zhang, L.; Yao, J.; Man, C.; Cheng, X.; Xiao, K.; Li, X. Mechanical properties and corrosion behavior of selective laser melted 316L stainless steel after different heat treatment processes. *J. Mater. Sci. Technol.* **2019**, *35*, 1499–1507. [CrossRef]
24. Kurzynowski, T.; Gruber, K.; Stopyra, W.; Kuznicka, B.; Chlebus, E. Correlation between process parameters, microstructure and properties of 316 L stainless steel processed by selective laser melting. *Mater. Sci. Eng. A* **2018**, *718*, 64–73. [CrossRef]
25. Lemke, J.N.; Casati, R.; Lecis, N.F.M.; Andrianopoli, C.; Varone, A.; Montanari, R.; Vedani, M. Design of wear-resistant austenitic steels for selective laser melting. *Metall. Mater. Trans. A* **2018**, *49*, 962–971. [CrossRef]
26. Lanzutti, A.; Marin, E.; Tamura, K.; Morita, T.; Magnan, M.; Vaglio, E.; Andreatta, F.; Sortino, M.; Totis, G.; Fedrizzi, L. High temperature study of the evolution of the tribolayer in additively manufactured AISI 316L steel. *Addit. Manuf.* **2020**, *31*, 101258. [CrossRef]
27. de Lima, M.S.F.; Sankaré, S. Microstructure and mechanical behavior of laser additive manufactured AISI 316 stainless steel stringers. *Mater. Des.* **2014**, *55*, 526–532. [CrossRef]
28. Pinto, F.C.; Souza Filho, I.R.; Sandim, M.J.R.; Sandim, H.R.Z. Defects in parts manufactured by selective laser melting caused by δ-ferrite in reused 316L steel powder feedstock. *Addit. Manuf.* **2020**, *31*, 100979. [CrossRef]
29. Lee, S.H. CMT-based wire arc additive manufacturing using 316L stainless steel: Effect of heat accumulation on the multi-layer deposits. *Metals* **2020**, *10*, 278. [CrossRef]
30. Marinelli, M.; Milani, E.; Montuori, M.; Paoletti, A.; Paroli, P.; Thomas, J. High-quality diamond grow by chemical-vapor deposition: Improved collection efficiency in α-particle detection. *Appl. Phys. Lett.* **1994**, *75*, 3216–3218. [CrossRef]
31. Cullity, B.D. *Elements of X-Ray Diffraction*, 2nd ed.; Addison Wesley Publishing Company INC.: Reading, MA, USA, 1977.
32. Ridley, N.; Stuart, H. Partial molar volumes from high-temperature lattice parameters of iron–carbon austenites. *Metal. Sci. J.* **1970**, *4*, 219–222. [CrossRef]
33. Stelmashenko, N.A.; Walls, M.G.; Brown, L.; Milman, Y.V. Microindentation on W and MO oriented single crystals: An STM study. *Acta Metall. Et Mater.* **1993**, *41*, 2855–2865. [CrossRef]
34. Ma, Q.; Clarke, D.R. Size dependent hardness in silver single crystals. *J. Mater. Res.* **1995**, *10*, 853–863. [CrossRef]
35. Jőnsson, B.; Hogmark, S. Hardness measurements of thin films. *Thin Solid Film.* **1984**, *114*, 257–269. [CrossRef]
36. Montanari, R.; Sili, A.; Costanza, G. Improvement of the fatigue behaviour of an Al6061/20%SiCp composite by means of titanium coatings. *Compos. Sci. Technol.* **2001**, *61*, 2047–2054. [CrossRef]
37. Costanza, G.; Montanari, R.; Quadrini, F.; Sili, A. Influence of Ti coatings on the fatigue behaviour of Al-matrix MMCs. Part I: Experimental analysis. *Compos. B* **2005**, *36*, 439–445. [CrossRef]
38. Liu, C.; Wang, J.H.; Weng, J. Growth of micro- and nanocrystalline dual layer composite diamond films by microwave plasma CVD: Influence of CO2 concentration on growth of nano-layer. *J. Cryst. Growth* **2015**, *410*, 30–34. [CrossRef]
39. Fendrych, F.; Taylor, A.; Peksa, L.; Kratochvilova, I.; Vlcek, J.; Rezacova, V.; Petrak, V.; Kluiber, Z.; Fekete, L.; Liehr, M.; et al. Growth and characterization of nanodiamond layers prepared using the plasma-enhanced linear antennas microwave CVD system. *J. Phys. D Appl. Phys.* **2010**, *43*, 374018. [CrossRef]
40. Higa, A.; Hatta, A.; Ito, T.; Toguchi, M.; Hiraki, A. Effect of CO_2 addition on diamond growth by DC arc plasma jet chemical vapour deposition. *J. Appl. Phys.* **1996**, *35*, 216–220. [CrossRef]

41. Lifshitz, Y.; Köhler, T.; Frauenheim, T.; Guzmann, I.; Hoffman, A.; Zhang, R.Q.; Zhou, X.; Lee, S.T. The mechanism of diamond nucleation from energetic species. *Science* **2002**, *297*, 1531–1533. [CrossRef]
42. Brescia, R.; Schreck, M.; Gsell, S.; Fischer, M.; Stritzker, B. Transmission electron microscopy study of the very early stages of diamond growth on iridium. *Diam. Relat. Mater.* **2008**, *17*, 1045–1050. [CrossRef]
43. Wang, C.S.; Chen, H.C.; Cheng, H.F.; Lin, I.N. Growth behavior of nanocrystalline diamond films on ultrananocrystalline diamond nuclei: The transmission electron microscopy studies. *J. Appl. Phys.* **2009**, *105*, 374018. [CrossRef]
44. Li, X.J.; He, L.L.; Li, Y.S.; Yang, Q. Revealing the nucleation mechanism of diamond film deposited on steel by high resolution transmission electron microscopy. *Diam. Relat. Mater.* **2019**, *92*, 100–108. [CrossRef]
45. Li, X.J.; He, L.L.; Li, Y.S.; Yang, Q. Diamond deposition on iron and steel substrates: A review. *Micromachines* **2020**, *11*, 719. [CrossRef] [PubMed]
46. Ferrari, A.C.; Robertson, J. Raman spectroscopy of amorphous, nanostructured, diamond-like carbon, and nanodiamond. *Phil. Trans. R. Soc. Lond. A* **2004**, *362*, 2477–2512. [CrossRef] [PubMed]
47. Dychalska, A.; Popielarski, P.; Frankow, W.; Fabisiak, K.; Paprocki, K.; Szibowicz, M. Study of CVD diamond layers with amorphous carbon admixture by Raman scattering spectroscopy. *Mater. Sci. Pol.* **2015**, *33*, 799–805. [CrossRef]